A study of the deep structure of the energy landscape of glassy polystyrene: the exponential distribution of the energy barriers revealed by high-field electron spin resonance spectroscopy

LETTER TO THE EDITOR

A study of the deep structure of the energy landscape of glassy polystyrene: the exponential distribution of the energy barriers revealed by high-field electron spin resonance spectroscopy

V Bercu[1,2,3]**, M Martinelli**[1]**, C A Massa**[1]**, L A Pardi**[1] **and D Leporini**[2,3,4,5]

[1] IPCF-CNR, I-56100 Pisa, Italy
[2] Dipartimento di Fisica 'Enrico Fermi', Università di Pisa, via F Buonarroti 2, I-56127 Pisa, Italy
[3] INFM UdR Pisa, via F Buonarroti 2, I-56127 Pisa, Italy
[4] INFM-CRS SOFT, Università di Roma La Sapienza, Piazzale Aldo Moro 2, I-00185, Roma, Italy

E-mail: dino.leporini@df.unipi.it

Abstract

The reorientation of one small paramagnetic molecule (spin probe) in glassy polystyrene (PS) is studied by high-field electron spin resonance spectroscopy at two different Larmor frequencies (190 and 285 GHz). The exponential distribution of the energy barriers for the rotational motion of the spin probe is unambiguously evidenced at both 240 and 270 K. The same shape for the distribution of the energy barriers of PS was evidenced by the master curves provided by previous mechanical and light scattering studies. The breadth of the energy barrier distribution of the spin probe is in the range of the estimates of the breadth of the PS energy barrier distribution. The evidence that the deep structure of the energy landscape of PS exhibits the exponential shape of the energy barrier distribution agrees with the results from extreme-value statistics (Bouchaud and Mezard 1997 *J. Phys. A: Math. Gen.* **30** 7997) and the trap model by Bouchaud and co-workers (1996 *J. Phys. A: Math. Gen.* **29** 3847, 2001 *Phys. Rev.* B **64** 104417).

1. Introduction

The study of glassy solid dynamics is a very active one [1, 2]. Here one is interested in the temperature range which is, on the one hand, well below the glass transition temperature T_g to be able to neglect the ageing effect and consider the glassy system as one with constant structure

[5] Author to whom any correspondence should be addressed.

and, on the other hand, high enough to be able to neglect the tunnelling effects governing the low-temperature anomalies of glasses. In this regime the dynamics is thermally activated in the substructures of the minima of the energy landscape accounting for various subtle degrees of freedom [3]. It has been shown that in a glass the temperature dependence of the energy barrier distribution $g(E)$ is only weakly temperature dependent [4, 5].

The shape of the energy barrier distribution $g(E)$ in glasses has been extensively investigated via experiments [2, 4–12], theories [13–20] and simulations [21]. Basically, two different distributions are usually recovered, the Gaussian distribution [2, 4–7, 9, 13, 15, 21] and the exponential distribution [9–11, 14, 16–20]. The convolution of these two distributions [22] as well as the truncated Levy flight, i.e. a power law with exponential cutoff, resembling the stretched exponential [12], were also considered.

It is interesting to relate $g(E)$ with the density of states, i.e. the distribution of the minima of the energy landscape. On the upper part of the landscape, being explored at high temperatures, the central limit theorem suggests that the density is Gaussian [13, 21]. At lower temperatures the state point is trapped in the deepest low-energy states which are expected to be exponentially distributed following general arguments on extreme-value statistics leading to the so-called Gumbel distribution [18]. Random energy models [13] and numerical simulations [20] support the conclusion. The barrier height E during the jump from one state with energy E_1 to another state with energy E_2 has been modelled by the linear combination $E = \alpha E_2 + (1-\alpha)E_1$ [19]. In the case of trap models ($\alpha = 0$) the minima and the energy barriers have the same distribution. This also holds true for annealed disorder and $\alpha > 0$ [17, 19]. Moreover, one notes that the linear combination of independent Gaussian variables is Gaussian too, and the linear combination of independent exponential variables has an exponential tail. All in all strict relations are expected between $g(E)$ and the density of states.

If the average trapping time τ before overcoming a barrier of height E at temperature T is governed by the Arrhenius law,

$$\tau = \tau_0 \exp(E/kT) \tag{1}$$

with k being Boltzmann's constant, the distribution of barrier heights induces a distribution of trapping times $\rho(\tau)$. The explicit form of $\rho(\tau)$ for a Gaussian distribution of barrier heights with width σ_E is the log-Gauss distribution (LGD)

$$\rho_{\text{LGD}}(\tau) = \frac{1}{\sqrt{2\pi\sigma^2}} \exp\left[-\frac{1}{2\sigma^2}\left(\ln\frac{\tau}{\tau_{\text{LGD}}}\right)^2\right]\frac{1}{\tau} \tag{2}$$

where $\sigma = \sigma_E/kT$ is the width parameter. $\rho(\tau)$ is maximum at τ_{LGD}. If the distribution of barrier heights is exponential with average height $\overline{E}$

$$g(E) = \frac{1}{\overline{E}}\exp\left(-\frac{E}{\overline{E}}\right) \tag{3}$$

$\rho(\tau)$ is expressed by the power-law distribution (PD)

$$\rho_{\text{PD}}(\tau) = \begin{cases} 0 & \text{if } \tau < \tau_{\text{PD}} \\ x\tau_{\text{PD}}^x \tau^{-(x+1)} & \text{if } \tau \geqslant \tau_{\text{PD}} \end{cases} \tag{4}$$

with $x = kT/\overline{E}$ and $\tau_{\text{PD}} = \tau_0$. If the width of the energy barrier distribution is vanishingly small, a single trapping (correlation) time (SCT) is found and both ρ_{LGD} and ρ_{PD} reduce to

$$\rho_{\text{SCT}}(\tau) = \delta(\tau - \tau_{\text{SCT}}). \tag{5}$$

The shape of $g(E)$ has usually been studied by measuring the different susceptibilities $\chi''(\nu)$ arising from either collective or single-particle response. If the susceptibility is followed

by a static distribution of activated relaxation times in the presence of a wide distribution $g(E)$ it follows [23]

$$\chi''(\nu) \propto T g(E), \qquad E = kT \ln(1/2\pi \nu \tau_0). \tag{6}$$

The above equation shows that the shape of $\chi''(\nu)$ yields the shape of $g(E)$. The conversion factor between the frequency and the energy scales is the unknown attempt frequency $1/\tau_0$, which is usually treated as one adjustable parameter to set both the width and the location of $g(E)$. The dielectric spectroscopy provides a convenient frequency range for recovering the full shape of $\chi''(\nu)$ and then of $g(E)$ [4, 5]. In other cases, e.g. light scattering [10] and mechanical relaxation [11], the accessible frequency range is limited, and $g(E)$ is recovered by building suitable master curves assuming the time–temperature superposition principle. Nuclear magnetic resonance (NMR) offers an alternative procedure for getting information on $g(E)$ by analysing the NMR lineshape in terms of two weighted components [2, 24]. However, an adjustable conversion factor between the frequency and the energy scales is also needed.

The use of suitable probes to investigate the secondary relaxations in glasses by NMR [2, 6, 22, 24], electron spin resonance (ESR) [25–27] and phosphorescence [28] studies is well documented. In spite of those efforts, the relation between the probe motion and the host dynamics is usually not obvious, with few exceptions which, notably, involved relatively small and nearly spherical probe molecules [26]. It was also noted that small molecules, e.g. xanthone and benzophenone, are more sensitive to shorter segmental motions occurring at lower temperatures [28].

During the last few years continuous-wave (CW) and pulsed high-field ESR (HF-ESR) techniques were developed involving large polarizing magnetic fields, e.g. $B_0 \cong 3T$ corresponding to Larmor frequencies about 95 GHz (W band) [29–31]. HF-ESR is widely used in solid-state physics [32], biology [33–37] and polymer science [38–41]. One major feature is the remarkable orientation resolution [41] due to increased magnitude of the anisotropic Zeeman interaction leading to a wider distribution of resonance frequencies [42, 43].

In the present paper one demonstrates that the rotational motion of suitable small guest molecules (spin probes), as detected by HF-ESR, is an effective probe sensing the energy barrier distribution $g(E)$ of glassy polystyrene (PS). The choice of PS was motivated by a number of studies of $g(E)$ by Raman [9] and light scattering [10] and mechanical relaxation [11] which evidenced its exponential form (equation (3)). The distribution of barriers to be surmounted by suitable probes in PS was also studied by NMR [22]. The secondary relaxations of PS were investigated by phosphorescent probes [28].

This letter is organized as follows. In section 2 the background on ESR is presented. Experimental details are given in section 3 and the results are discussed in section 4. The conclusions are summarized in section 5.

2. ESR background

The main broadening mechanism of the ESR lineshape is the coupling between the reorientation of the spin probe and the relaxation of the electron magnetization **M** via the anisotropy of the Zeeman and the hyperfine magnetic interactions. When the molecule rotates, the coupling gives rise to fluctuating magnetic fields acting on the spin system. The resulting phase shifts and transitions relax the magnetization and broaden the resonance [42, 43]. Because of the roughness of the energy landscape and the highly branched character of the free volume distribution, one expects that the small spin probe undergoes jump dynamics in glasses. One efficient numerical approach for calculating the ESR line shape in the presence of rotational jumps is detailed elsewhere [39].

The rotational correlation time τ_c, i.e. the area below the correlation function of the spherical harmonic $Y_{2,0}$, is [25]

$$\tau_c = \frac{\tau^*}{\left[1 - \frac{\sin(\frac{5\phi}{2})}{5\sin(\frac{\phi}{2})}\right]} \tag{7}$$

where ϕ and τ^* are the size of the angular jump and the mean residence time before a jump takes place, respectively. In the limit $\phi \ll 1$ the jump model reduces to the isotropic diffusion model with $\tau_c = 1/6D = \tau^*/\phi^2$, where D is the rotational diffusion coefficient.

The occurrence of a static distribution of correlation times in glasses suggests evaluating the ESR line shape $L(B_0)$, which is usually detected by sweeping the static magnetic field B_0 and displaying the first derivative, as a weighted superposition of different contributions:

$$L(B_0) = \int_{-\infty}^{+\infty} d\tau_c \, L(B_0, \tau_c)\rho(\tau_c) \tag{8}$$

where $L(B_0, \tau_c)$ is the EPR line shape of the spin probes with correlation time τ_c and $\rho(\tau_c)$ is the τ_c distribution.

It must be pointed out that in the presence of a wide distribution of correlation times the ESR lineshape (equation (8)) cannot be simplified as a sum of few leading components. This is rather different with respect to NMR, where 'two-phase spectra' stemming from 'fast' and 'slow' molecules are observed [2]. If, on one hand, that feature leads to more elaborated numerical work, on the other hand it ensures that the ESR lineshape exhibits a much richer variety of detail, being markedly affected by the spin-probe dynamics which provides helpful constraints to the fit procedures and results in an improved information content of the spectra.

3. Experimental details

The PS was obtained from Aldrich and used as received. The weight-average molecular weight is $M_w = 230$ kg mol^{-1} and $T_g = 367$ K. The free radical used as spin probe was 2,2,6,6-tetramethyl-1-piperidinyloxy (TEMPO) from Aldrich. TEMPO has one unpaired electron spin $S = 1/2$ subject to hyperfine interaction with the nitrogen nucleus with spin $I = 1$. The sample was prepared by the solution method [44] by dissolving TEMPO and PS in chloroform. The solution was transferred onto the surface of a glass slide and heated at $T_g + 10$ K for 24 h. The spin probe concentration was less than 0.08% in weight. Appreciable broadening of the ESR line shape due to the spin–spin interaction is observed for concentrations larger than 0.2% in weight. No segregation of the spin probe was evidenced. Samples aged at room temperature for six months exhibited no appreciable change of the ESR lineshape.

The ESR experiments were carried out on the ultrawide-band ESR spectrometer which is detailed elsewhere [45]. In the present study the spectrometer was operated at two different frequencies: 190 and 285 GHz. The multi-frequency approach ensures better accuracy for determining the spin-probe dynamics. The sample of about 0.8 cm^3 was placed in a Teflon sample holder in a single-pass probe cell. All spectra were recorded and stored in a computer for off-line analysis.

4. Results and discussion

The numerical simulation of the ESR lineshape relies greatly on the accurate determination of the magnetic parameters of the spin probe. To this aim, one profited from the enhanced resolution of HF-ESR and measured the ESR lineshape of TEMPO in PS at low temperature
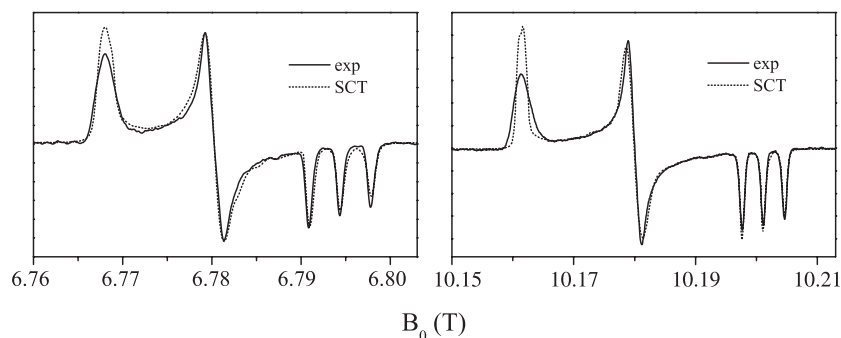
Figure 1. The ESR line shapes at 190 GHz (left) and 285 GHz (right) of TEMPO in PS at 50 K. The magnetic parameters are: $g_x = 2.009\,94 \pm 3 \times 10^{-5}$, $g_y = 2.006\,28 \pm 3 \times 10^{-5}$, $g_z = 2.002\,12 \pm 3 \times 10^{-5}$, A_x (mT) $= 0.62 \pm 0.02$, A_y (mT) $= 0.70 \pm 0.02$, A_z (mT) $= 3.40 \pm 0.02$. The superimposed dashed curves are best fits according to the SCT model, equation (5), with $\tau_{SCT} = 25$ ns (190 GHz) and $\tau_{SCT} = 19$ ns (285 GHz). The jump angle $\phi = 60°$. The theoretical lineshapes were convoluted by a Gaussian with width $w = 0.15$ mT to account for the inhomogeneous broadening.

where the rotational motion of the spin probe is very slow and the resulting lineshape approaches the so-called 'powder' or 'rigid' limit lineshape [43]. The results at 50 K are shown in figure 1. It is seen that the lineshapes at both the operating frequencies are well fitted by the SCT model with a single set of magnetic parameters. The small discrepancy between the simulation and the lineshape at low magnetic field was already noted in other studies [30]. Remarkably, no distribution of correlation times is evidenced at 50 K. At this stage a complete discussion of this finding needs a detailed investigation of the temperature dependence of the rotational dynamics of TEMPO in PS. This is beyond the purpose of the present letter and will be discussed thoroughly in a forthcoming paper [46].

Figure 2 compares the ESR lineshapes at 190 GHz of TEMPO in PS at $T = 270$ K $= T_g - 97$ K with the SCT (left, two adjustable parameters τ_{SCT}, ϕ) and LGD models (right, three adjustable parameters τ_{LGD}, ϕ and σ). For a given jump angle ϕ the remaining one (SCT) or two (LGD) parameters have been adjusted. It is apparent that the SCT model is inadequate. Large disagreements were also found when fitting the ESR lineshape at 285 GHz (not shown). Figure 2 shows that the LGD model yields better agreement for large jump angles. However, closer inspection reveals deviations in the wings of the ESR lineshapes at both low and high field. The ESR absorption of these regions is mainly contributed by spin probes with their x molecular axis (low field) or z axis (high field) being parallel to the static magnetic field [41]. The magnetic parameters of the spin probe being precisely measured, it may be shown that the above disagreements are clear signatures of the overestimate of the jump angle size [46]. The best-fit value of the width parameter $\sigma = 1$ of the LGD distribution (equation (2)) corresponds to the width $\sigma_E/k = 270$ K of the energy barrier distribution of TEMPO in PS. Rössler and co-workers found by NMR $\sigma_E/k = 276$ K for hexamethylbenzene in PS in the temperature range roughly 150–300 K [22]. Even if TEMPO and hexamethylbenzene have similar sizes their shape is rather different, so it is quite reassuring to note that the rotational motion of different *small* probes investigated by different techniques lead to comparable results.

Figure 3 compares the PD model (equation (4), three adjustable parameters τ_{PD}, ϕ and x) with the ESR lineshape at both 190 and 285 GHz of TEMPO in PS at 270 K. Again, having fixed the jump angle, one adjusted the other two parameters. It is clearly seen that the agreement is quite improved, especially for small jump angles. Figure 4 provides the same comparison at 240 K for the case $\phi = 20°$ which results in the best agreement. From figures 3 and 4 it
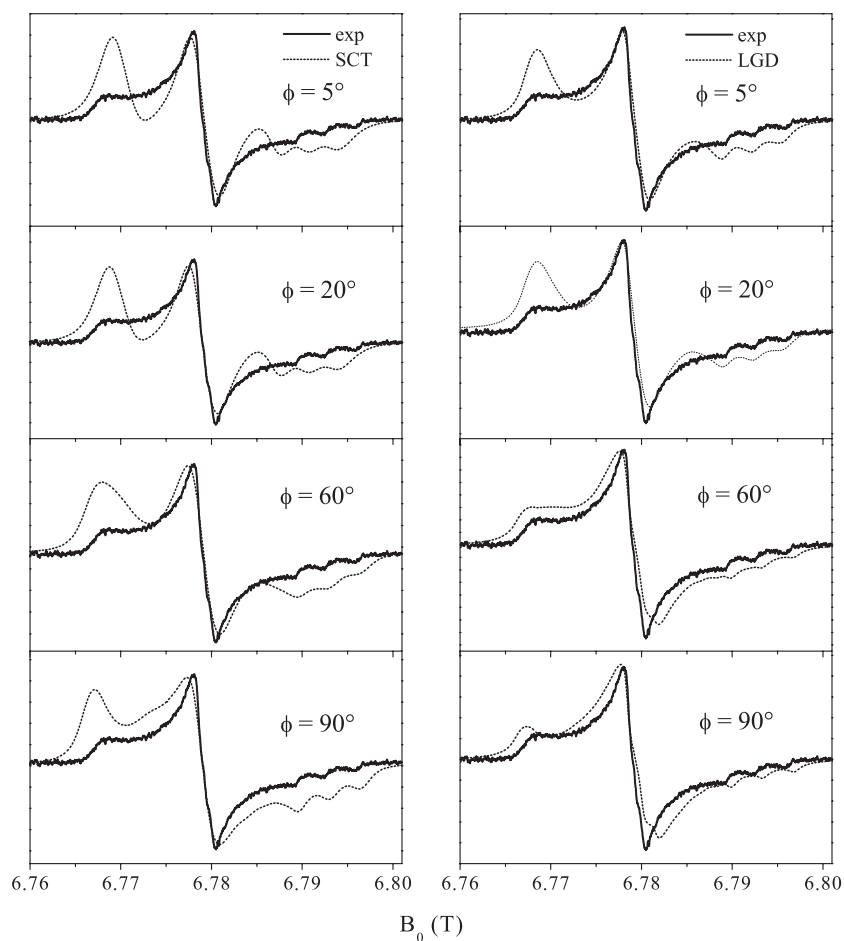
Figure 2. Comparison of the EPR line shape at 190 GHz of TEMPO in PS at 270 K with SCT and LGD models. The magnetic parameters and Gaussian width are as in figure 1. Left: best fits according to the SCT model, equation (5), with different jump angles. The best-fit parameters are: $\phi = 5°$, $\tau_{SCT} = 4.2$ ns; $\phi = 20°$, $\tau_{SCT} = 4.16$ ns; $\phi = 60°$, $\tau_{SCT} = 3.75$ ns; $\phi = 90°$, $\tau_{SCT} = 3.16$ ns. Right: best fits according to the LGD model, equation (2), with different jump angles. The best-fit value of the width was found to be independent of the jump angles and set to $\sigma = 1.0$. The other best-fit parameters are: $\phi = 5°$, $\tau_{LGD} = 3.6$ ns; $\phi = 20°$, $\tau_{LGD} = 3.6$ ns; $\phi = 60°$, $\tau_{LGD} = 1.8$ ns; $\phi = 90°$, $\tau_{LGD} = 1.6$ ns.

is seen that at both 240 and 270 K the best-fit value of τ_{PD} is different for the two operating frequencies 190 and 285 GHz with $\tau_{PD}(190\,\text{GHz}) < \tau_{PD}(285\,\text{GHz})$. The uncertainty on τ_{PD} is roughly less than 20%. Constraining τ_{PD} to having the same value at 190 and 285 GHz in the fit procedure results in larger deviations between the experimental lineshape and the numerical results. The decrease of τ_{PD} with the operating ESR frequency has been noted by us also at frequencies lower than 190 GHz and will be discussed elsewhere [46]. Without going into details, it has to be ascribed to the relation between the Larmor period (roughly the inverse of the operating frequency) and the sensitivity of the ESR spectroscopy to the fast rotational dynamics.

Table 1 summarizes the best-fit results of the PD model ($\phi = 20°$) for both 190 and 285 GHz. The width of the barrier height distribution of TEMPO in PS is in the range
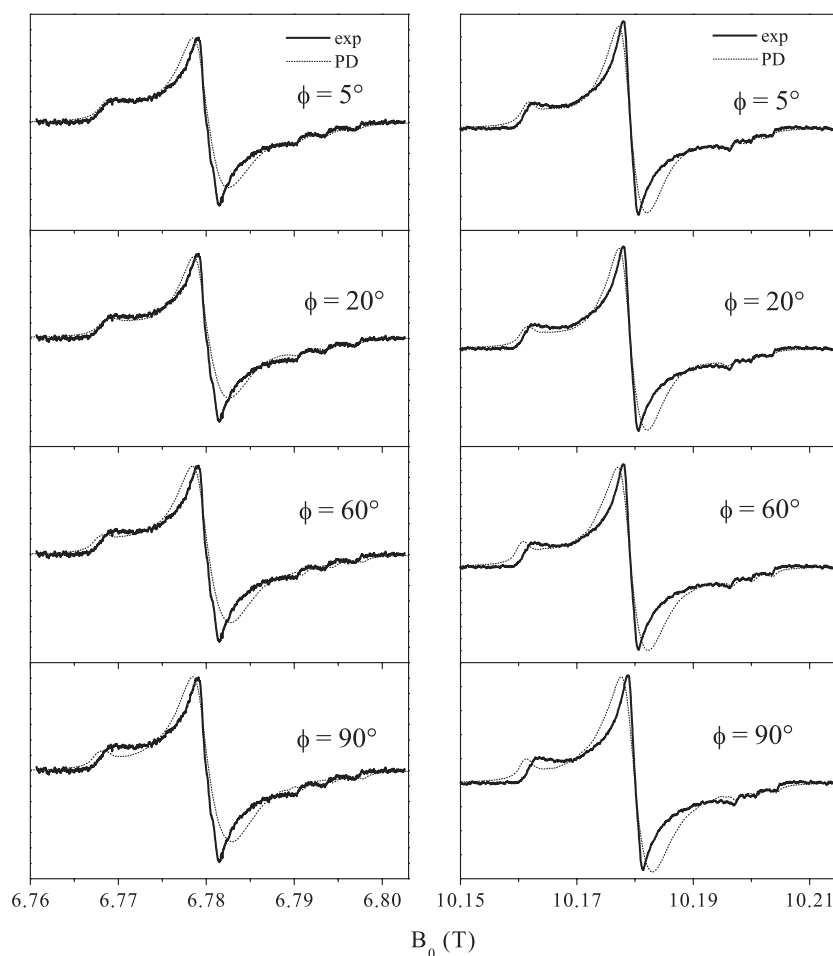
Figure 3. Best fits of the EPR line shape at 190 GHz (left) and 285 GHz (right) of TEMPO in PS at 270 K according to the PD model, equation (4), and different jump angles ϕ. The magnetic parameters and Gaussian width are as in figure 1. The best-fit parameters are as follows. Left: $\phi = 5°, x = 0.6, \tau_{PD} = 0.24$ ns; $\phi = 20°, x = 0.575, \tau_{PD} = 0.225$ ns; $\phi = 60°, x = 0.6, \tau_{PD} = 0.25$ ns; $\phi = 90°, x = 0.63, \tau_{PD} = 0.25$ ns. Right: $\phi = 5°, x = 0.52, \tau_{PD} = 0.13$ ns; $\phi = 20°, x = 0.5, \tau_{PD} = 0.13$ ns; $\phi = 60°, x = 0.5, \tau_{PD} = 0.15$ ns; $\phi = 90°, x = 0.55, \tau_{PD} = 0.15$ ns.

$470\,\text{K} \leqslant \overline{E}/k \leqslant 705\,\text{K}$. One may wonder if this range corresponds to correlation times which are effectively accessed by HF-ESR in that the longest correlation time of TEMPO which may be measured is $\tau_{max} \cong 100$ ns. To this aim, one estimates the maximum energy barrier which TEMPO may overcome leading to appreciable motional narrowing effects in the lineshape as $E_{max} \cong kT \ln(\tau_{max}/\tau_{PD})$. In the temperature range 240–270 K we get $E_{max}/k \cong 1500$–$1800\,\text{K}$, which is considerably larger than $\overline{E}$; see table 1. This confirms that the overall ESR lineshape, expressed by the superposition given by equation (8), is mostly due to components which are motionally narrowed to some or a large extent by the reorientation of TEMPO. Table 1 shows that the width of the barrier height distribution of TEMPO in PS increases on cooling. This points to better coupling of TEMPO and PS at $T \cong 240$ K. However, we recall that at lower temperatures the width decreases (see figure 1). This non-monotonic behaviour, as well as the
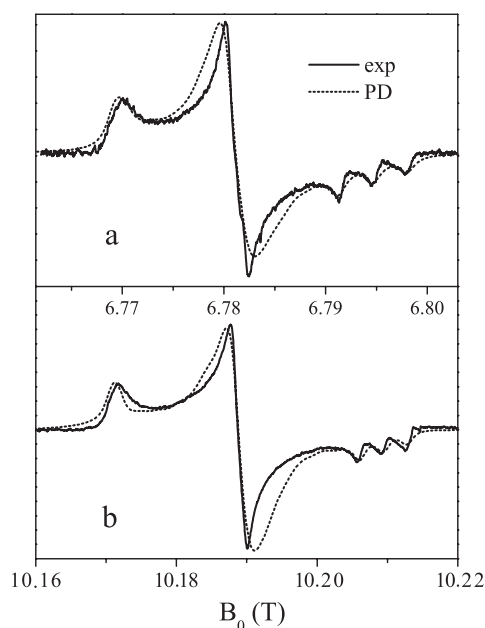
Figure 4. The ESR line shapes at $T = 240$ K and frequencies 190 GHz (panel a) and 285 GHz (panel b). The dotted superimposed curves are numerical simulations by using the PD model (equation (4)) with $x = 0.4$, $\tau_{PD} = 0.25$ ns (panel a); $x = 0.34$, $\tau_{PD} = 0.12$ ns (panel b). In both cases the best-fit value of the jump angle is $\phi = 20°$. The magnetic parameters and Gaussian width are as in figure 1.

Table 1. The width of the exponential distribution of barrier heights $\overline{E}$ of TEMPO in PS at $T = 240$ and 270 K as provided by the best fit of the HF-ESR lineshapes at 190 and 285 GHz by using the PD model with jump angle $\phi = 20°$. Previous measurements of the width of the distribution of barrier heights of PS by internal friction [11], Raman [9] and light scattering [10] yield $\overline{E}_{IF}/k = 760 \pm 40$ K, $\overline{E}_{Raman}/k = 530 \pm 60$ K and $\overline{E}_{LS}/k = 530 \pm 40$ K, respectively.

T (K)	f (GHz)	$\overline{E}/k$ (K)
240	190	600 ± 36
240	285	705 ± 42
270	190	470 ± 28
270	285	540 ± 32

increase of $\overline{E}$ with the frequency which is also apparent in table 1, will be discussed in detail elsewhere [46].

The exponential distribution (equation (3)) of the barrier heights of PS was evidenced by both internal friction [11], Raman [9] and light scattering [10] measurements. The studies converted the mechanical [11] and the optical [9, 10] susceptibilities $\chi''(\nu)$ by equation (6) to get $g(E)$ and estimated its width as $\overline{E}_{IF}/k = 760 \pm 40$ K, $\overline{E}_{Raman}/k = 530 \pm 60$ K and $\overline{E}_{LS}/k = 530 \pm 40$ K, respectively. It was concluded that, in spite of the different estimates of $\overline{E}$, the corresponding three patterns of $g(E)$ are in good agreement (see [10] and especially figure 4 from that paper). Table 1 shows that the width of the barrier height distribution of TEMPO is in the range of the estimates on the width of the PS distribution provided by the above studies.

One final remark concerns τ_{PD}, i.e. the time scale τ_0 of the activated trapping of TEMPO, equation (1). The best-fit values of τ_0 are about 120–250 ps (see the captions of figures 3, 4). Previous studies on the rotational dynamics of TEMPO in several glassy polymers were carried out by the customary X-band ESR spectroscopy at 9 GHz and analysed in terms of the SCT model [47, 48]. They yielded $\tau_0 \cong 10^2$–10^3 ps. In particular, for TEMPO in glassy PS it was found $\tau_0 \cong 10^2$ ps [47].

5. Conclusions

The rotational motion of the guest molecule TEMPO in PS was investigated by using HF-ESR at two different Larmor frequencies (190 and 285 GHz). The use of a single correlation time (SCT model) was found to be inadequate to fit the ESR lineshape. Limited improvement was reached by considering a Gaussian distribution of energy barriers for TEMPO (LGD model) even if the best-fit width compared rather well with the one of molecular probes with similar size in PS as measured by NMR studies [22]. Assuming the exponential shape of the energy barrier distribution for the spin probe (PD model) led to much better agreement at both 240 and 270 K. The same shape was also evidenced by other studies [9–11] on the distribution of the energy barriers of PS which reported considerably different estimates of the width $\overline{E}$ ($>40\%$). The width of the barrier height distribution of TEMPO was found to be in the range of the previous estimates of $\overline{E}$ for PS.

The evidence that the deep structure of the energy landscape of PS exhibits the exponential shape of the energy barrier distribution agrees with the results from extreme-value statistics [18] and the trap model by Bouchaud and co-workers [17, 19].

References

[1] Angell C A, Ngai K L, McKenna G B, McMillan P F and Martin S W 2000 *J. Appl. Phys.* **88** 3113
[2] Böhmer R, Diezemann G, Hinze G and Rössler E 2001 *Prog. Nucl. Mag. Reson.* **39** 191
[3] Angell C A 1998 *Nature* **393** 521
[4] Wu L 1991 *Phys. Rev.* B **43** 9906
[5] Wu L and Nagel S R 1992 *Phys. Rev.* B **46** 11198
[6] Qi F, Böhmer R and Sillescu H 2001 *Phys. Chem. Chem. Phys.* **3** 4022
[7] Vogel M and Rössler E 2001 *J. Chem. Phys.* **114** 5802
[8] Vogel M and Rössler E 2001 *J. Chem. Phys.* **115** 10883
[9] Sokolov A P, Novikov V N and Strube B 1997 *Europhys. Lett.* **38** 49
[10] Surovtsev N V, Wiedersich J A H, Novikov V N, Rössler E and Sokolov A P 1998 *Phys. Rev.* B **58** 14888
[11] Topp K A and Cahill D G 1996 *Z. Phys.* B **101** 235
[12] Gorham N T, Woodward R C, St Pierre T G, Stamps R L, Walker M J, Greig D and Matthew J A D 2004
        J. Appl. Phys. **95** 6983
[13] Derrida B 1981 *Phys. Rev.* B **24** 2613
[14] Scher H and Montroll E W 1975 *Phys. Rev.* B **12** 2455
[15] Bässler H 1987 *Phys. Rev. Lett.* **58** 767
[16] Odagaki T 1995 *Phys. Rev. Lett.* **75** 3701
[17] Monthus C and Bouchaud J-P 1996 *J. Phys. A: Math. Gen.* **29** 3847
[18] Bouchaud J-P and Mezard M 1997 *J. Phys. A: Math. Gen.* **30** 7997
[19] Rinn B, Maass P and Bouchaud J-P 2001 *Phys. Rev.* B **64** 104417
[20] Schön J C and Sibani P 2000 *Europhys. Lett.* **49** 196
[21] Denny R A, Reichman D R and Bouchaud J-P 2003 *Phys. Rev. Lett.* **90** 025503
[22] Rössler E, Taupitz M and Vieth H M 1990 *J. Phys. Chem.* **94** 6879
[23] Böttcher C J F and Bordewijk P 1978 *Theory of Electric Polarization* (Amsterdam: Elsevier)
[24] Rössler E, Taupitz M, Börner K, Schulz M and Vieth H M 1990 *J. Chem. Phys.* **92** 5847

[25] Andreozzi L, Cianflone F, Donati C and Leporini D 1996 *J. Phys.: Condens. Matter* **8** 3795

[26] Faetti M, Giordano M, Leporini D and Pardi L 1999 *Macromolecules* **32** 1876

[27] Barbieri A, Gorini G and Leporini D 2004 *Phys. Rev.* E **69** 061509

[28] Christoff M and Atvars T D Z 1999 *Macromolecules* **32** 6093

[29] Ondar M A, Grinberg O Y, Oranskii L G, Kurochkin V I and Lebedev Y L 1981 *J. Struct. Chem.* **22** 626

[30] Budil D E, Earle K A and Freed J H 1993 *J. Phys. Chem.* **97** 1294

[31] Schweiger A and Jeschke G 2001 *Principles of Pulse Electron Paramagnetic Resonance* (Oxford: Oxford University Press)

[32] Martinelli M, Massa C A, Pardi L A, Bercu V and Popescu F F 2003 *Phys. Rev.* B **67** 014425

[33] Liang Z C and Freed J H 1999 *J. Phys. Chem.* B **103** 6384

[34] Liang Z C, Freed J H, Keyes R S and Bobst A M 2000 *J. Phys. Chem.* B **104** 5373

[35] Borbat P P, Costa-Filho A J, Earle K A, Moscicki J K and Freed J H 2001 *Science* **291** 266

[36] Fuchs M R, Schleicher E, Schnegg A, Kay C W M, Torring J T, Bittl R, Bacher A, Richter G, Mobius K and Weber S 2002 *J. Phys. Chem.* B **106** 8885

[37] Schafer K O, Bittl R, Lendzian F, Barynin V, Weyhermuller T, Wieghardt K and Lubitz W 2003 *J. Phys. Chem.* B **107** 1242

[38] Pilar J, Labsky J, Marek A, Budil D E, Earle K A and Freed J H 2000 *Macromolecules* **32** 4438

[39] Leporini D, Zhu X X, Krause M, Jeschke G and Spiess H W 2002 *Macromolecules* **35** 3977

[40] Leporini D, Schädler V, Wiesner U, Spiess H W and Jeschke G 2002 *J. Non-Cryst. Solids* **307–310** 510

[41] Leporini D, Schädler V, Wiesner U, Spiess H W and Jeschke G 2003 *J. Chem. Phys.* **119** 11829

[42] Berliner L J (ed) 1976 *Spin Labeling: Theory and Applications* (New York: Academic)
Berliner L J and Reuben J (ed) 1989 *Biological Magnetic Resonance* vol 8 (New York: Plenum)

[43] Muus L T and Atkins P W (ed) 1972 *Electron Spin Relaxation in Liquids* (New York: Plenum)

[44] Saalmueller J W, Long H W, Volkmer T, Wiesner U, Maresch G G and Spiess H W 1996 *J. Polym. Sci.* B **34** 1093

[45] Annino G, Cassettari M, Fittipaldi M, Lenci L, Longo I, Martinelli M, Massa C A and Pardi L A 2000 *Appl. Magn. Reson.* **19** 495

[46] Bercu V, Pardi L A, Massa C A, Martinelli M and Leporini D 2004 to be submitted

[47] Törmälä P 1980 *Molecular Motion in Polymers by ESR* ed R F Boyer and S E Keinath (Chur: Harwood)

[48] Cameron G G 1982 *Pure Appl. Chem.* **54** 483